49th AIAA Aerospace Sciences Meeting including the New Horizons Forum and Aerospace Exposition
4 - 7 January 2011, Orlando, Florida

AIAA 2011-68

Unstart of a Supersonic Model Inlet/Isolator Flow Induced by Mass Injection

*H. Do[1], *S. Im[2], *§M. G. Mungal[3] and *M. A. Cappelli[4]
*Mechanical Engineering Department, Stanford University, Stanford, CA 94305
§School of Engineering, Santa Clara University, Santa Clara, CA 95053

A transverse jet is injected into a supersonic model inlet/isolator flow to induce unstart. Planar Laser Rayleigh Scattering (PLRS) from condensed CO_2 particles is used to visualize the unsteady flow during unstart. Pressure traces are recorded using high speed pressure sensors located in the bottom wall of the tunnel. A series of time sequence PLRS images reveals that an unstart shock originates near the jet injection nozzle and propagates upstream, unstarting the inlet flow upon its arrival at the inlet lip. Studies conducted over a range of model configurations indicate that the presence of turbulent wall boundary layers strongly affect the unstart dynamics. It is found that relatively thick turbulent boundary layers in asymmetric wall boundary layer configurations prompt the formation of unstart shocks whereas symmetric boundary layer conditions lead to the formation of pseudo-shocks. Both cases facilitate fast inlet unstart when compared to cases in which there are initially relatively thin laminar boundary layers.

Nomenclature

γ	=	ratio of specific heats
Ma, M	=	Mach number
p	=	static pressure
p_0	=	stagnation pressure
ρ	=	density
R	=	square root of the ratio of the jet momentum flux to that of the free stream
T_0	=	stagnation temperature
u	=	flow velocity

I. Introduction

INLET unstart has been described as the disgorgement of a shock system at the inlet throat of a scramjet/ramjet engine.[1] If not avoided, it can cause in-flight engine malfunctioning.[2-9] In 1966, a hybrid engine (turbojet and ramjet) powered air fighter (SR-71 Blackbird) capable of Mach 3.2 flight at 80,000 ft crashed due to engine cutoff induced by this inlet unstart.[7] Most frequently occurring during the transition to ramjet/scramjet mode in the flight Mach number ranges of 3 to 6,[10] unstart is believed to be caused by the thermal choking[11] of the internal supersonic flow triggered by increased heat release in the combustor.[12-14] The heat release in the combustor is followed by a pressure rise in the inlet duct and boundary layer separation/growth, reducing the core flow area, and forcing the internal flow into a subsonic regime.[15] Recently, in a ground test facility that mimics the thermal choking by the downstream movement of a mechanical flap, Wagner et al.[8,9,16] confirmed the presence of the separated boundary layer using Particle Image Velocimetry (PIV), and captured (via high speed Schlieren photography) the formation and dynamics of an unstart shock system that interacted with the boundary layers. The propagation speed of this unstart shock has been characterized by several researchers, and was determined from wall pressure measurements

---

[1] Postdoctoral Researcher, Mechanical Engineering, Stanford University, non-Member.
[2] PhD Candidate, Mechanical Engineering, Stanford University, AIAA Student Member.
[3] Dean of Engineering, Santa Clara University, Professor Emeritus, Mechanical Engineering, Stanford University, AIAA Associate Fellow.
[4] Professor, Mechanical Engineering, Stanford University, non-Member.

to be in the range of 10 – 27 m/s in the studies of Wieting,[2] 55 – 70 m/s in the studies of Rodi et al.,[4] and, more recently by Wagner et al.,[16] in the range of 19 – 80 m/s.

Past studies have examined methods such as boundary layer bleeding,[14] the introduction of isolators[13,17-19] and vortex generator jets,[20] as a means of avoiding or delaying inlet unstart. All of these methods seek to influence the evolution of the boundary layer during the upstream propagation of flow disturbances that originate from the combustor. Recording and understanding the dynamics of boundary layer evolution during unstart is critical to the development of such unstart mitigation strategies. Studies will therefore require diagnostic methods that are capable of resolving the structure of boundary layers, and shock-boundary layer interactions.

This paper describes a study of the unstart phenomenon in a supersonic inlet, triggered by mass injection downstream of the inlet. The jet/supersonic flow and ensuing dynamics are highly three-dimensional, and we visualize the unstart flow features (e.g. boundary layers, shock-boundary layer interactions) using Planar Laser Rayleigh Scattering (PLRS) from condensed CO_2 particles (particulate fog). Miles and Lempert,[21] Wu et al.,[22] and Poggie et al.[23] have demonstrated the general utility of this diagnostic for low temperature/pressure supersonic flows expanded through the diverging nozzle of a supersonic wind tunnel of low (ambient) stagnation temperature. Weak (e.g., oblique) shocks are visualized as demarcations in intensity as a result of the post-shock increase in density (and hence particles). However, regions of elevated temperature can cause particle sublimation, and therefore boundary layers and regions behind strong (normal) shocks lack particles and appear dark, with very strong contrasts. While qualitative at this time, this diagnostic captures flow features with high spatial discrimination (unlike Schlieren photography, which is line-of-sight), and reveals flow dynamics suitable for quantitative characterization, e.g., of regions of boundary layer transition, slip lines, and the propagation of both weak and strong shockwaves.

The use of this PLRS visualization technique allows us to investigate the evolution of fine scale flow structures under unstart flow conditions produced in a model inlet built into a supersonic wind tunnel.[24] The current study reveals that the flow features emerging during unstart are influenced by wall boundary layer conditions, which, in some cases, can either delay or accelerate the inlet unstart process.

II. Experimental Setup

The experimental facility consists of a Ma = 5 in-draft wind tunnel, an integrated laser system and a jet injection module.

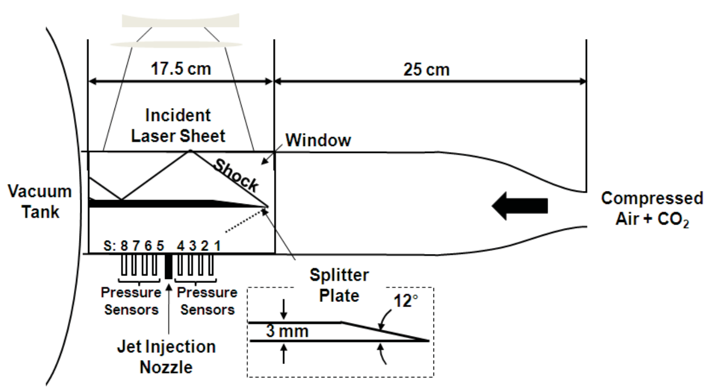

Figure 1. *Experimental setup including a Mach 5 wind tunnel, pressure sensors and PLRS imaging system.*

A schematic of the Ma = 5 wind tunnel is shown in Fig. 1. High pressure air (p_0 = 350 kPa and T_0 = 300 K) containing CO_2 (approximately 25 % by volume) expands through a converging/diverging nozzle (25:1 area ratio) to establish a relatively uniform Ma = 5 flow in a rectangular test section (4 cm × 4 cm cross-sectional area). The exit of the tunnel is connected to a vacuum tank that accommodates the incoming mass flow for approximately 5 seconds of run time. During this run time, the vacuum tank pressure is maintained at values lower than the static pressure in the test section. A honeycomb panel 2.5 cm in length comprising 3 mm hexagonal cells is placed upstream of the converging nozzle to suppress flow swirling, mostly generated at various junctions in the gas stream inlet piping. The static pressure and temperature of the flow in the test section is approximately 1 kPa and 50 K, respectively.

Windows on both sides of the test section and transparent upper/lower walls allow optical access. A 3 mm thick splitter plate (aluminum plate), having a sharp leading wedge and a transparent slot of an embedded acrylic plate divides the test section into two parts of equal cross sectional area. The sharp leading wedge of an asymmetric design (12° angled wedge in the top half of channel), as shown in Fig. 1, is used to generate a relatively shock-free flow in the lower half (Case I) while it causes a shock train in the upper half. In the base configuration (Case I) shown in Fig. 1, the jet (ID = 3 mm) is injected through a relatively thick boundary layer (which originated upstream

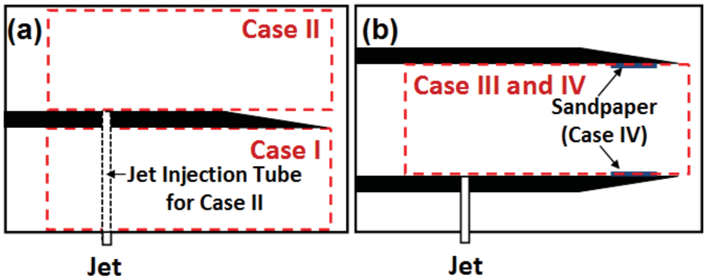

Figure 2. *The region of interest in each case (Case I through Case IV) and configurations of the splitter plates.*

near the throat of the tunnel) into the flow through the model inlet/isolator flow defined in the lower half of the tunnel. The boundary layer on the upper wall of this inlet (i.e. on the splitter plate) grows naturally from the leading edge of the plate. Three other model inlet/isolator configurations are studied. All four of the configurations are summarized in Fig. 2, which also depicts the flow regions imaged by planar Rayleigh scattering (indicated qualitatively by the rectangles defined by the dashed lines).

Static pressure traces on the bottom wall of the tunnel are recorded using eight fast response (100 kHz) pressure sensors (S1 – S8: PCB Piezotronics, Model 113A26). This provides measurements of the temporal evolution in pressure on the lower wall of the Case I model inlet/isolator flow configurations. At this time, this is the only configuration for which we have pressure data The sensors and the jet injection nozzle, placed between S4 and S5, are separated by 15 mm along the centerline of the bottom wall parallel to the freestream flow direction: S1 and S8 are located 60 mm upstream and downstream from the nozzle, respectively. The distance between the tip of the splitter plate (270 mm downstream from the converging/diverging nozzle throat) and the jet nozzle is 75 mm.

The experimental components for Rayleigh scattering include a Nd:YAG laser (New Wave, Gemini PIV) capable of generating approximately 100 mJ/pulse (532 nm wavelength) energy with 10 Hz pulse repetition, an unintensified CCD camera (La Vision, Imager Intense) and a computer (not shown) to facilitate data acquisition. The laser beam is transformed into a thin sheet of 0.5 mm thickness to illuminate the test section using a combination of two concave cylindrical lenses and a convex spherical lens. Scattered light is captured by the camera along a direction normal to the laser sheet. Laser firing is synchronized with the CCD camera exposure (3 μs shutter). One of the laser pulses is selected to trigger the jet injection module while the tunnel is operating, but delayed as desired by a pulse delay generator (SRS, DG 535) to take time resolved images at different phases in the flow evolution induced by the jet injection. The jet injection is controlled by a solenoid valve (ASCO, Red Hat II) driven by a controller (Optimal Engineering System Inc.) receiving the trigger signal from the delay generator. A sonic jet (air, in these studies presented here) is injected into the test section through a 3 mm diameter hole in the bottom wall resulting in a flow disturbance and an overall increase in flow pressure and temperature. Relevant to the jet interaction and mixing with the supersonic free stream is the square root of the ratio of the jet momentum flux to that of the free stream, defined by:

$$R = \sqrt{\frac{(\rho u^2)_{jet}}{(\rho u^2)_\infty}} = \sqrt{\frac{(\gamma p M^2)_{jet}}{(\gamma p M^2)_\infty}}$$

Here, ρ, u, γ, p, and M are air density, velocity, ratio of specific heats, pressure and Mach number of the jet (subscript *jet*) and freestream (subscript ∞) flow, respectively. For our results described here, R is approximately 4.5.

III. Results

A. Unstart

Unstart induced by air jet injection is clearly reflected in the pressure traces measured on the bottom surface of the wind tunnel (Case I). Figure 3 (a) documents the sudden pressure rise at the various locations on the lower wall following the jet injection through the nozzle located between S4 and S5. The time reference (t = 0 sec) in this figure corresponds to when the pressure first rises at the sensor located at S8 (i.e., the farthest downstream region characterized). The pressure at S8 starts to rise abruptly at approximately 10 ms after the jet injection trigger signal opens the solenoid valve. Absolute pressure offsets are subtracted from the traces to illustrate relative differences between the pressure recorded before and after the jet injection. The pressure traces recorded at the locations nearest to the jet nozzle (S4 and S5, not shown) fluctuate significantly, due to flow instabilities in the near field of the jet. It is noteworthy that the first pressure increase is recorded at S8 and this high pressure region then expands towards the

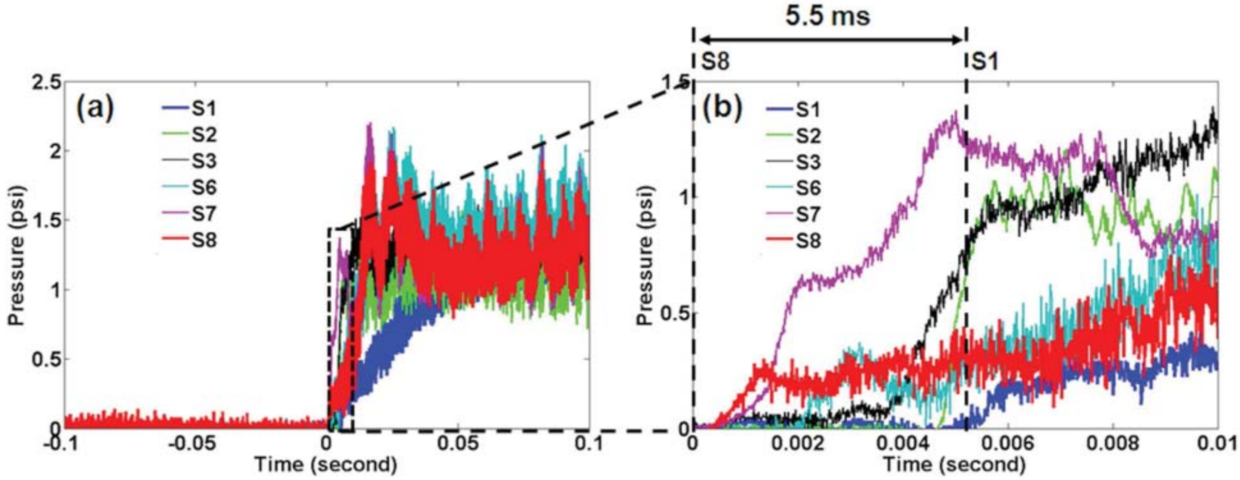

Figure 3. *Pressure traces recorded on the bottom wall of the wind tunnel.*

upstream region of the tunnel, presumably along the subsonic boundary layer, in succession through to the location at S1 (Fig. 3 (b)). This ordering in the rise in pressure confirms that unchoking originates downstream of the jet injection point, triggering tunnel unstart, i.e., a transition to a subsonic flow regime. We conjecture that the unchoked flow, i.e. the subsonic flow caused by the mass injection, first appears far downstream near the model exit due to the reduced supersonic core flow area by the growth of boundary layers on the tunnel surfaces and the increment of mass flow rate by the jet injection. The propagation of this high pressure region from S8 to S1 (over 12 cm distance) takes approximately 5.5 ± 0.5 ms (see Fig. 3 (b)) indicating that that this pressure wave propagates at a speed of approximately 22 ± 2 m/s (a mean of 4 measurements). For comparison the freestream speed is approximately 720 m/s.

B. Asymmetric Wall Boundary Layer Conditions

Here, we discuss the model inlet unstart dynamics induced by a jet injection with model configurations designated in Fig. 2, as Case I and Case II. These cases are referred to here as having *asymmetric* wall boundary conditions, in that they are primarily distinguished by the presence of either a thick turbulent boundary layer (Case I) or a thin laminar boundary layer (Case II) on the inlet wall through which the jet is injected. Under the current flow condition, the model inlet is found to unstart 20 ms and 25 ms after the jet is triggered, for Case I and Case II respectively.

Numerous studies have shown that the unstart shock is a critical flow feature in understanding the transient unstart phenomenon.[2,4,8,9,16,24] As discussed below, a comparison of Cases I and II provides evidence for the significant role played by the presence of a turbulent boundary layer in prompting the formation of the unstart shock. The time sequence PLRS images in Figs 4 and 5 illustrates the evolution in the flow features while the flow undergoes unstart induced by an air jet of R = 4.5. The entire flow region of interest (designated by the dashed rectangular region in Fig. 2) is interrogated in two separate Rayleigh scattering frames. The first frame illuminates the region in the vicinity of the jet nozzle (Fig. 4), and the other, an upstream region near the tip of the splitter plate (Fig. 5). Each imaging region covers a 5 cm width along the freestream flow direction (from right to the left) and an 18.5 mm height. When combined, these two frames span the region within the dashed rectangular lines for Case I or Case II, in Fig. 2(a).

The unstart process with the base configuration (Case I), as described in detail in a previous paper,[24] is discussed briefly here again, and depicted in Figs 4 (a) and 5 (a). The figures reveal that the boundary layer growth/separation on the bottom wall of the inlet (also the bottom wall of the tunnel), initiated by the jet injection, propagates upstream (seen between 13 ms (Fig. 4 (a)) and 17 ms (Fig. 5 (a)) after jet triggering) and produces an oblique unstart shock first appearing in front of the jet in the 13 ms panel of Fig. 4 (a). This shock propagates forward, and the inlet flow unstarts shortly after the arrival of this shock at the inlet (Fig. 5 (a), 17 ms). Concurrently, we also see a separated flow on the upper wall (Fig. 4(a), 12 ms) when the jet-induced bow shock interacts with this thin boundary layer. This upper wall disturbance also propagates upstream, preceding the unstart shock, and arrives at the tip of the splitter plate at 13.5 ms (Fig. 5 (a)). It is trailed by a rapidly growing boundary layer that appears to become turbulent within one inlet duct height downstream distance.

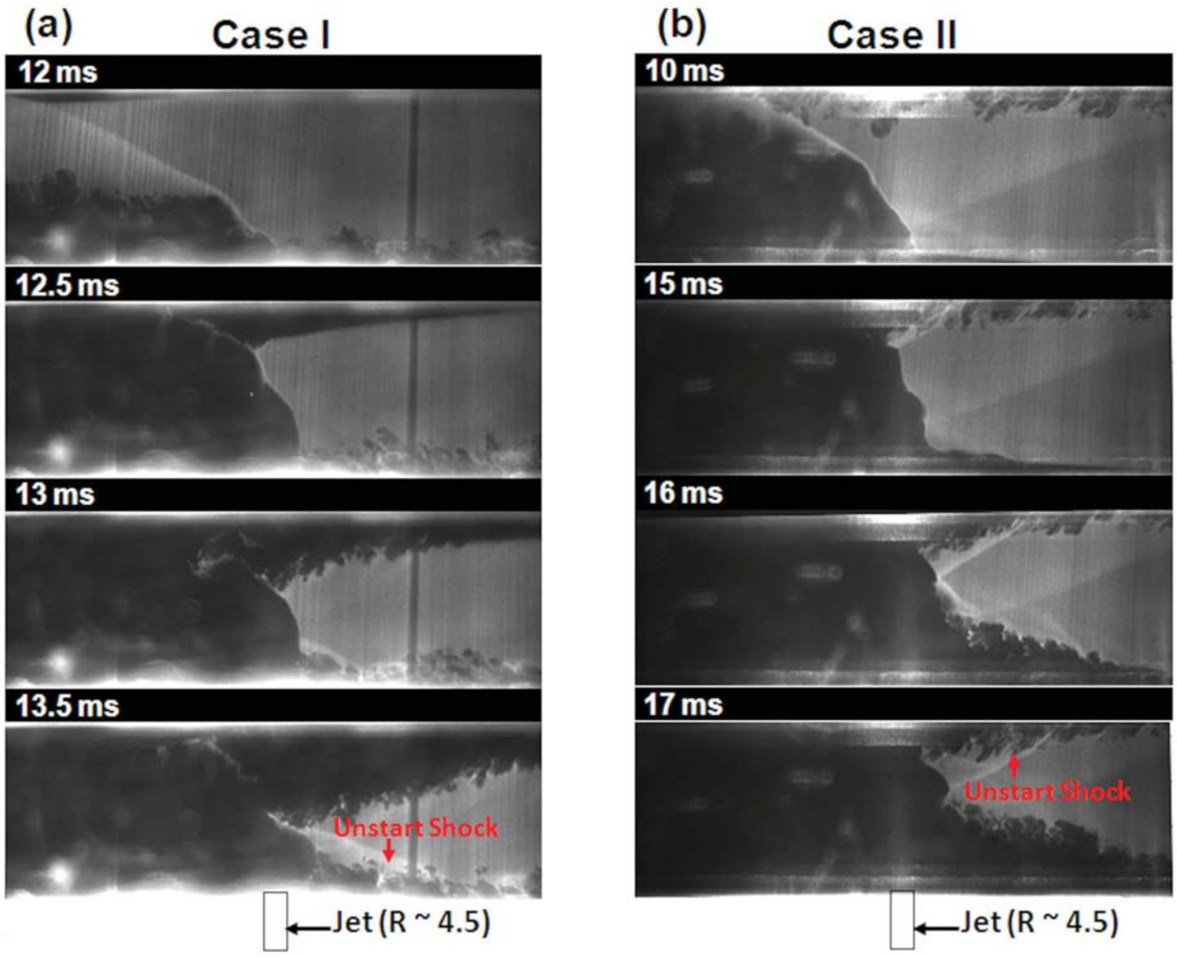

Figure 4. *Time sequential PLRS images taken in the adjacent to the jet with the configurations of (a) Case I and (b) Case II.*

Several flow structures, such as the formation and evolution of the unstart shock, separated flow regions and developing boundary layers seen for Case II (Fig. 4(b) and 5(b)) appear to be very similar to those seen in Case I (Fig 4(a) and 5(a)), particularly apparent if the images of Case II are flipped vertically. Shortly following the injection we see the emergence of a separated flow just upstream of the jet on the initially thin laminar boundary layer (first emerging on the bottom at 10 ms in Fig. 4 (b)). As in Case I, this separated flow appears to propagate upstream, and is followed by the growth of a thick turbulent boundary layer/separated flow, reaching the wedged region of the splitter tip at 20 ms (Fig. 5 (b)). Surprisingly, the unstart shock, is spawned on the opposite surface at a time of about 15 ms (Fig. 4 (b)), and moves upstream between 15 ms (Fig. 4 (b)) and 24.5 ms (Fig. 5 (b)) along the surface. Here, it is noteworthy that, in both Cases I and II, the unstart shock emerges on the surface where there is initially (prior to the jet injection) a thick turbulent boundary layer, suggesting that this thick turbulent boundary layer prompts the formation of this oblique unstart shock. Note that qualitatively, the same flow features appear, albeit at different times in each case, e.g. the unstart shock emerges at 13 ms in Case I (Fig. 4 (a)) and 15 ms in Case II (Fig. 4 (b)). This 2 ms difference may be attributed to several factors, such as the longer jet gas delivery tube in Case II (which possibly delays jet development), the different wall boundary conditions where the jet is discharged (Case I is turbulent, Case II is laminar), and/or the pressure disturbances caused by incident shocks, presumably stronger in Case II with the wedged inlet lip.

C. Symmetric Wall Boundary Layer Conditions

We have seen in Sec. B that while wall boundary conditions (asymmetric, i.e., one wall turbulent, the other laminar) affect the transient unstart flow features, injecting either through a turbulent or laminar boundary layer is not found to cause significant differences in the overall time to unstart the inlet flow. In this section, we describe the *symmetric* inlet flow configurations, Cases III and IV (Fig. 2 (b)), which provide the same wall boundary conditions

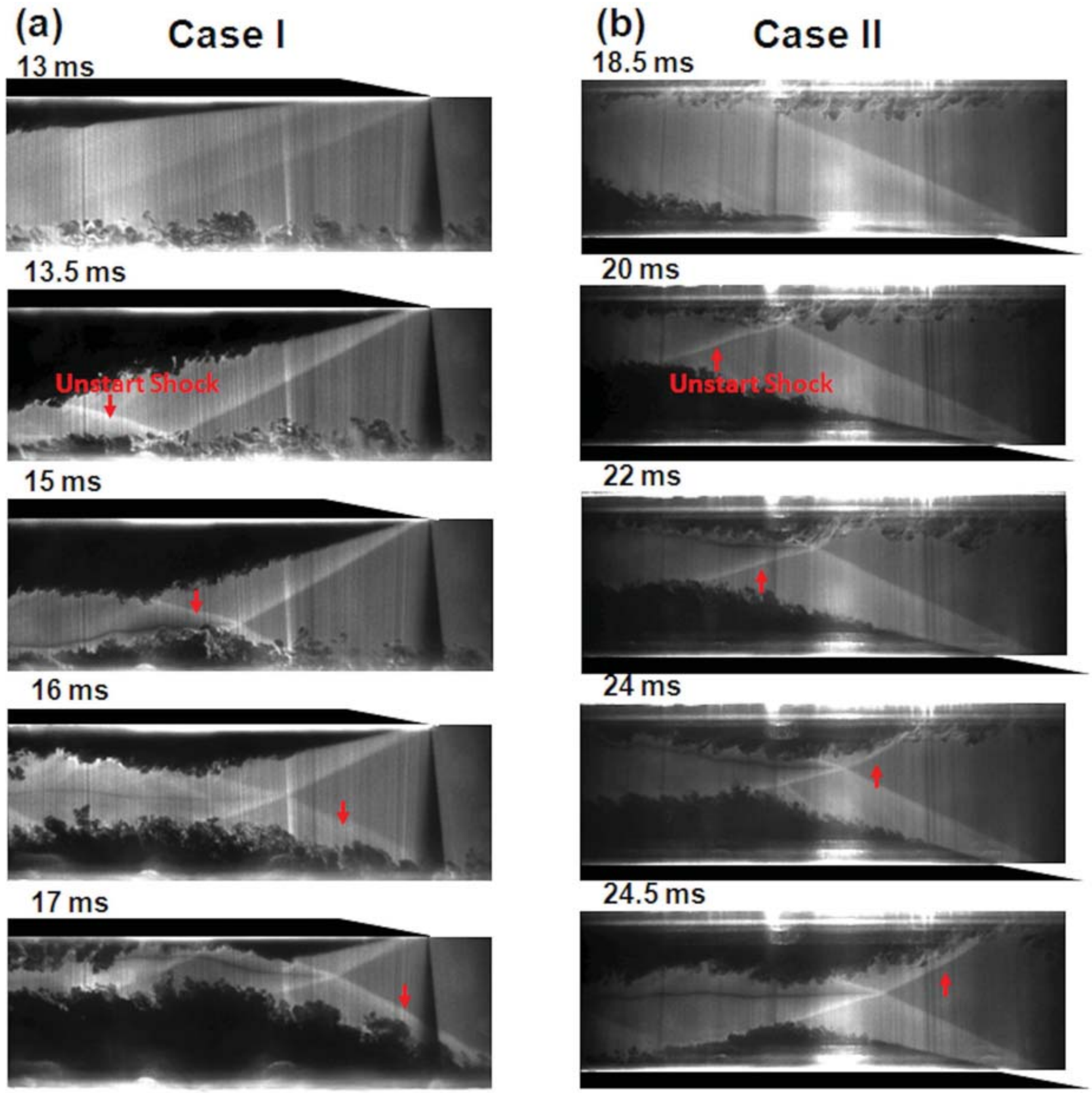

Figure 5. *Time sequential PLRS images covering the first 5 cm region downstream of the splitter tip taken with the configurations of (a) Case I and (b) Case II.*

on the top and bottom walls of the model inlet flow. For Case III, both boundary layers are thin and initially laminar, while in Case IV both walls have relatively thick turbulent boundary layers prior to jet injection.

We find that with the Case III configuration, the oblique unstart shock that was seen to emerge in Case I and II *does not appear,* and, as a consequence, inlet flow unstart is significantly delayed in comparison with these other cases. Figure 6 presents the Rayleigh scattering images for the two frames spanning the entire region of interest, depicting the inlet flow observed for Case III over a time ranging from prior to jet injection through to flow unstart, at a time of 55 ms after jet triggering. As shown in Fig. 6 (a), (taken in the absence of the jet), the two splitter plates (with wedge outward facing) isolate the main flow from the turbulent boundary layers on the tunnel walls to define the model inlet. In this configuration, thin (initially laminar) boundary layers form on both upper and lower walls. Weak shock waves appear originating from the splitter tips, most likely due to the small but finite dimensions of the tips. Note that the interaction of the shock originating from the lower wall induces flow separation on the upper wall, at a downstream location of approximately 40 mm. The flow is seen to undergo a laminar-to-turbulent flow transition, with the clear indication of relatively thin turbulent boundary layers in the downstream frame. Figure 6(b)

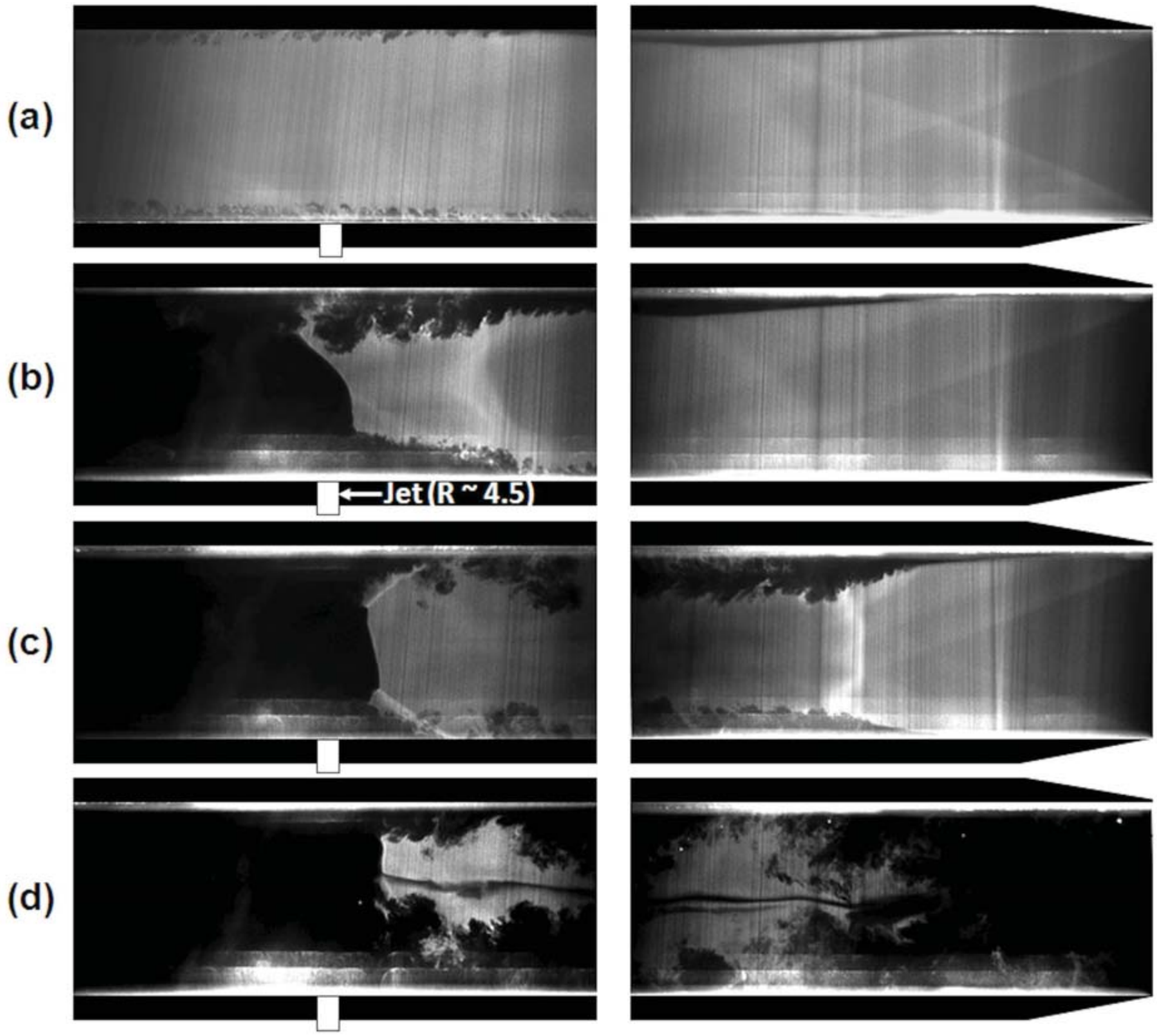

Figure 6. *PLRS images with Case III configuration: (a) before the jet injection (b) the formation of a compression wave (16 – 17 ms after the jet injection), (c) a dual-shock structure (an upstream pseudo-shock and a downstream shockwave) seen in the time duration of 18 – 55 ms, and (d) breakdown of the dual-shock structure at 55 ms.*

is a similar depiction, taken after jet injection (approximately 17 ms after jet triggering). At this time, we see from the brighter region that spans across the inlet at approximately 20 mm upstream of the jet, that a compression wave (presumably a pseudo-shock) forms, almost normal to the flow direction, as indicated by the diffuse, brighter signal at the center of the channel. This compression is followed by the apparent thickening of the turbulent boundary layers on both top and bottom surfaces. This compression wave propagates upstream and arrives at a position of about 27 mm from the splitter tip within about 1 ms (see Fig. 6(c)) remaining there for approximately 37 ms (from 18 ms to 55 ms). This wave is thicker than typical shockwaves such as the oblique unstart shock seen in Cases I and II, or the incident shocks originating from the splitter tips, and is not strong enough to cause transition to subsonic flow. This is evident from the fact that we still see significant Rayleigh scattering off of CO_2 fog behind this wave, as this fog would be expected to evaporate in subsonic flow regions. In addition, we see from Fig. 6(c) what appears to be a normal shock (little can be said about this with the present diagnostic) or the emergence of a symmetric lambda shock downstream of this compression wave, just upstream of the jet.

So-called pseudo-shocks are often observed in internal flows[25-27] and seem to accompany the growth of turbulent boundary layers when a supersonic flow decelerates to a subsonic flow in a duct. Arai et al.[25] observed experimentally that a series of pseudo-shocks intermittently pressurize and decelerates a supersonic flow in a square duct and boundary layers were found to thicken abruptly behind the first pseudo-shock, in ways consistent with what

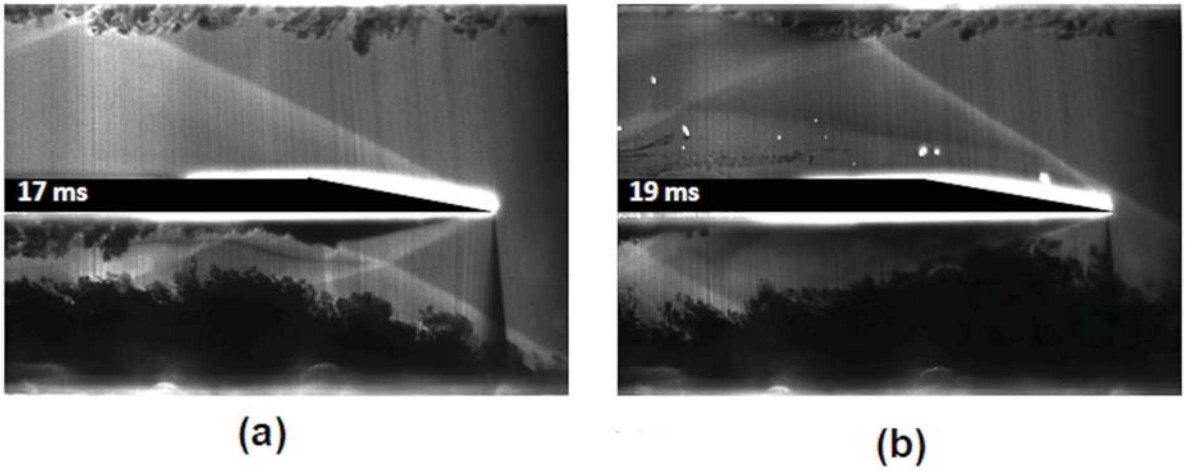

Figure 7. *PLRS images revealing that the unstart shock propagates further upstream out of the imaging region in Case I.*

we observed here in Figs. 6 (b) and 6 (c). In numerical simulations, Hataue[26] predicted a flow structure in a duct that consisted of an upstream pseudo-shock together with a downstream shock that produced a subsonic flow. The downstream shock was strongly deformed by the interaction with the now thickened boundary layers (lambda shock). This "dual-shock" (pseudo-shock followed by a strong shock) structure appears to be qualitatively similar to that shown in Fig. 6 (c).

A sudden breakdown of this dual-shock structure leading to inlet flow unstart is observed (see Fig. 6(d)) at a

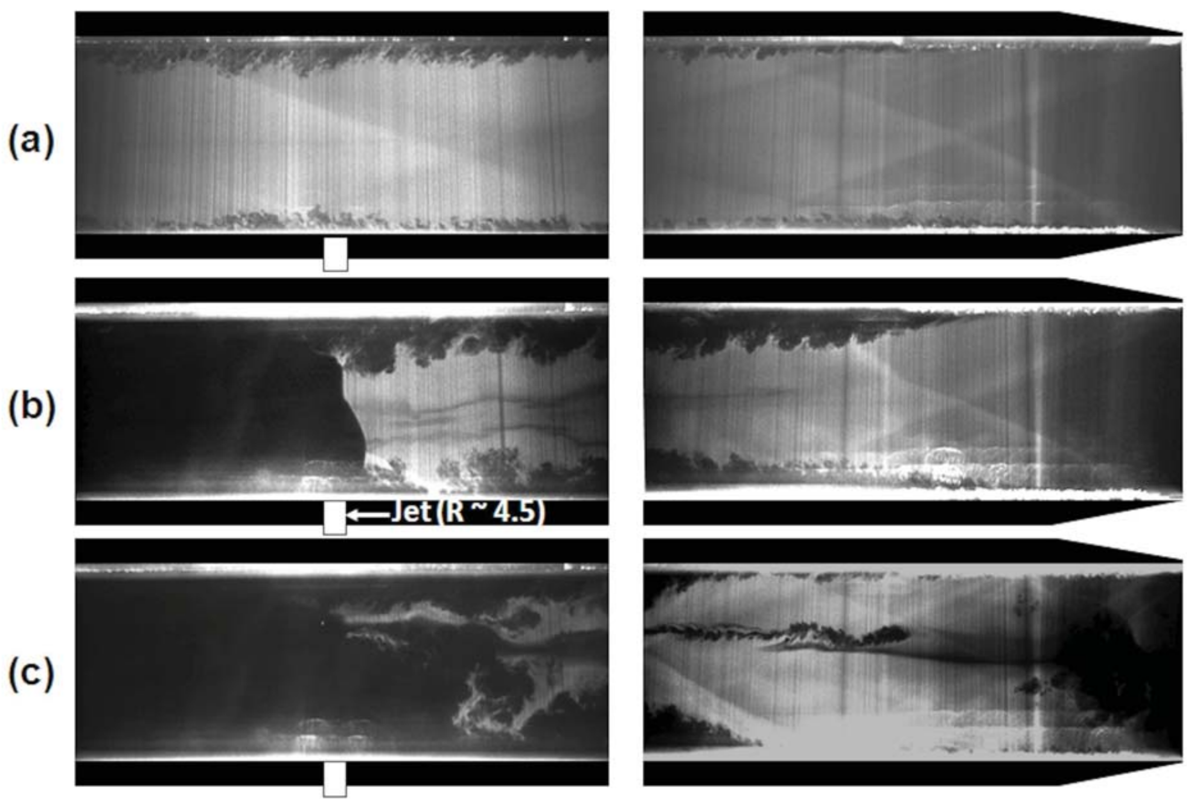

Figure 8. *PLRS images with Case IV configuration: (a) before the jet injection, (b) shockwaves intersecting each other at the inlet and standing steady during 16 – 24 ms, and (c) tunnel unstart at 25 ms.*

time of 55 ms ± 0.5 ms. The breakdown occurs swiftly, within 1 ms. It is noteworthy that, in Case III, it therefore takes about 55 ms for the inlet flow to unstart – a time that is significantly longer than that of the previous two cases discussed (20 ms (Case I) and 25 ms (Case II)). Inlet unstart appears to be delayed by the isolating of inlet flow from the thick turbulent boundary layer on the tunnel walls. At this time, however, the physics related to the sudden breakdown of the flow structure is not resolved. We believe that this breakdown is caused by the relatively slow build-up in pressure behind the upstream pseudo-shock. This mechanism will be examined in the future studies in which pressure measurements will be made along the inlet walls of the isolated flow.

From the observations made with the Case III configuration, it appears that pre-existing thick turbulent boundary layers on the tunnel wall prompt the formation of the unstart shock seen in the Case I and II configurations. In the Case I and II studies, this thick turbulent boundary layer is a nascent feature of the tunnel flow, growing along the tunnel wall (which serves as one wall defining the inlet) and originating in the throat region of the converging-diverging nozzle, far upstream of the inlet lip. This thick boundary layer provides a subsonic region that can possibly channel the propagation of downstream flow (e.g., pressure) disturbances into the region upstream of the inlet lip. For example, the unstart shock in Case I can propagate far upstream beyond the splitter plate edge, as shown in Fig. 7. The foot of the unstart shock on the bottom wall is beyond the image field in the 17 ms panel (Fig. 7 (a)) and continues to propagate further upstream at 19 ms (Fig. 7 (b)), where it now disturbs the flow in the upper half of the tunnel, reducing the Mach number as confirmed by the increase in the incident shock angle (Fig. 7 (b)). This makes a direct comparison of the later stages of unstart in Case III with Cases I and II difficult, because, as shown in Fig. 7, the turbulent boundary layer on the tunnel walls (in Cases I and II) result in an unstart shock that disrupts the upstream flow region before the complete unstart of the inlet flow – a situation not encountered in Case III.

Case IV (same geometrical configuration of Case III) also isolates the inlet from this thick turbulent boundary layer, but generates its own relatively thick turbulent wall boundary layers by the use of sandpaper near the leading edge of the splitter plates. Figure 8 (a) reveals the presence of turbulent boundary layers developing on the walls generated by sandpaper attached 5 mm downstream of the plate tips. An earlier complete inlet unstart (25 ms) compared to that seen in Case III (55 ms), is observed with this configuration. This unstart is about as fast as that seen in Case I (20 ms) and II (25 ms), although the general flow features are more similar to those seen for Case III. A compression wave (just behind the intersection of the two incident shocks), accompanying the development of thick turbulent boundary layers, propagates upstream to a quasi-stable position, anchoring there for 8 ms (16 ms – 24 ms after jet triggering), as seen in Fig. 8 (b). Then, a sudden break down of this flow structure (dual-shock) is observed at 25 ms (Fig. 8 (c)) instantly followed by complete inlet flow unstart. We attribute this early unstart, in comparison to that of Case III, to the initial turbulent boundary layers on the upper and lower inlet walls.

IV. Summary

An in-draft Mach 5 wind tunnel was used to generate approach flow conditions for studies of unstart in model inlet/isolator flows. In the studies described, inlet unstart is generated by the injection of an air jet. Flow dynamics following jet injection were investigated with four different inlet configurations.

Planar Laser Rayleigh Scattering imaging was used to characterize flow features, including the evolution of boundary layers and shocks. We find that unstart flow features and the overall inlet unstart process are strongly affected by the characteristics of the initial wall boundary layer prior to jet injection. In asymmetric inlet configurations, with a thick turbulent boundary layer on one wall, and a thin (initially laminar) boundary layer on the other, an unstart shock emerges, but only on the wall with an initially thick turbulent boundary layer, independent of the boundary layer through which the jet is injected. In either case, complete unstart of the inlet occurs within about 25 ms. With symmetric wall configurations (i.e., cases in which wall boundary layer are similar on both sides, either turbulent or laminar), there is no oblique unstart shock. Instead, we see a relatively weak compression wave or pseudo-shock, which initially propagates upstream in advance of unstart, and remains quasi-stable for some time, until a catastrophic breakdown in the structure occurs and the inlet flow unstarts completely. The duration over which this pseudo-shock is anchored in the inlet depends on the nature of the initial boundary layer (thin laminar, or thick turbulent). With relatively thin (initially laminar) boundary layers, the pseudo-shock appears stable until 55 ms following jet injection – more than twice as long as the case in which the initial boundary layers are tripped to be turbulent (25 ms). The time for unstart in the turbulent symmetric condition is comparable to that of the asymmetric cases.

Acknowledgments

This work is sponsored by the Department of Energy sponsored Predictive Science Academic Alliance Program (PSAAP) at Stanford University.

References

[1]Emami S., Trexler C. A., Auslender A. H., and Weidner J. P., "Experimental investigation of inlet-combustor isolators for a dual-mode scramjet at a Mach number of 4," NASA Technical Paper 3502, 1995.

[2]Wieting A. R., "Exploratory study of transient unstart phenomena in a three-dimensional fixed-geometry scramjet engine," NASA TN D-8156, 1976.

[3]Hawkins W. R. and Marquart E. J., "Two-dimensional Generic Inlet Unstart Detection at Mach 2.5–5.0," *6th International Aerospace Planes and Hypersonics Technologies Conference*, AIAA, Washington, DC, 1995, AIAA 95-6016.

[4]Rodi P. E., Emami S., and Trexler C. A., "Unsteady Pressure Behavior in a Ramjet/scramjet Inlet," *Journal of Propulsion and Power*, Vol. 12, No. 3, 1996, pp. 486-493.

[5]Shimura T., Mitani T., Sakuranaka N., and Izumikawa M., "Load Oscillations Caused by Unstart of Hypersonic Wind Tunnels and Engines," *Journal of Propulsion and Power*, Vol. 14, No. 3, 1998, pp. 348-353.

[6]O'Byrne S., Doolan M., Olsen S. R., and Houwing A. F. P., "Analysis of Transient Thermal Choking Processes in a Model Scramjet Engine," *Journal of Propulsion and Power*, Vol. 16, No. 5, 2000, pp. 808-814.

[7]Graham R. H., *SR-71 Blackbird*, MBI Publishing Company, St. Paul, MN, 2002, pp. 27-28.

[8]Wagner J. L., Yuceil K. B., Valdivia A., Clemens N. T., and Dolling D. S., "PIV Measurements of the Unstart Process in a Supersonic Inlet/isolator," *38th Fluid Dynamics Conference and Exhibit*, AIAA, Washington, DC, 2008, AIAA 2008-3849.

[9]Wagner J. L., Yuceil K. B., and Clemens N. T., "PIV Measurements of Unstart of an Inlet-Isolator Model in a Mach 5 Flow," *39th Fluid Dynamics Conference and Exhibit*, AIAA, Washington, DC, 2009, AIAA 2009-4209.

[10]Andreadis D. "Scramjet Engines Enabling the Seamless Integration of Air & Space Operations," The Industrial Physicist, Aug/Sept, 2004.

[11]Mashio S., Kurashina K., Bamba T., Okimoto S., and Kaji S., "Unstart Phenomenon due to Thermal Choke in Scramjet Module," *AIAA/NAL-NASDA-ISAS 10th International Space Planes and Hypersonic Systems and Technologies Conference*, AIAA, Washington, DC, 2001.

[12]Heiser W. H.and Pratt D. T., *Hypersonic Air Breathing Propulsion: AIAA Education Series*, AIAA, Washington, DC, 1993.

[13]Sato S., Izumikawa M., Tomioka S., and Mitani T., "Scramjet Engine Test at Mach 6 Flight Condition," *33rd AIAA/ASME/SAE/ASEE Joint Propulsion Conference and Exhibit*, AIAA, Washington, DC, 1997, AIAA 97-3021.

[14]Kodera M., Tomioka S., Kanda T., Mitani T., and Kobayashi K., "Mach 6 Test of a Scramjet Engine with Boundary-layer Bleeding and Two-staged Fuel Injection," *12th AIAA International Space Planes and Hypersonic Systems and Technologies*, AIAA, Washington, DC, 2003, AIAA 2003-7049.

[15]McDaniel K. S. and Edwards J. R., "Three-Dimensional Simulation of Thermal Choking in a Model Scramjet Combustor," *39th Aerospace Sciences Meeting and Exhibit*, AIAA, Washington, DC, 2001, AIAA 2001-0382.

[16]Wagner J. L., Yuceil K. B., Valdivia A., Clemens N. T., and Dolling D. S., "Experimental Investigation of Unstart in an Inlet/isolator Model in Mach 5 Flow,"*AIAA Journal*, Vol. 47, No. 6, 2009, pp. 1528-1542.

[17]Curran E. T., Heiser W. H., and Pratt D. T., "Fluid Phenomena in Scramjet Combustion Systems," *Annual Review of Fluid Mechanics,* Vol. 28, 1996, pp. 323-360.

[18]Wang X. and Le J. "Computations of Inlet/isolator for SCRAMjet Engine," *Journal of Thermal Science*, Vol. 9, issue 4, 2000, pp. 334-338.

[19]Tam C., Eklund D., and Behdadnia R., "Influence of Downstream Boundary Conditions on Scramjet-isolator Simulations," *26th AIAA Applied Aerodynamics Conference*, AIAA, Washington, DC, 2008, AIAA 2008-6929.

[20]Valdivia A., Yuceil K. B., Wagner J. L., Clemens N. T., and Dolling D. S., "Active Control of Supersonic Inlet Unstart Using Vortex Generator Jets," *39th Fluid Dynamics Conference and Exhibit*, AIAA, Washington, DC, 2009, AIAA 2009-4022.

[21]Miles R. B. and Lempert W. R., "Quantitative Flow Visualization in Unseeded Flows," *Annual Review of Fluid Mechanics*, Vol. 29, 1997, pp. 285-326.

[22]Wu P., Lempert W. R., and Miles R. B., "Megahertz Pulse-burst Laser and Visualization of Shock-wave/boundary-layer Interaction," *AIAA Journal* Vol. 38, No. 4, 2000, pp. 672-679.

[23]Poggie J., Erbland P. J., Smits A. J, and Miles R. B., "Quantitative Visualization of Compressible Turbulent Shear Flows Using Condensate-enhanced Rayleigh Scattering," *Experiments in Fluids*, Vol. 37, 2004, pp. 438-454.

[24]Do H., Im S., Mungal M.G., and Cappelli M. A., "Visualizing Supersonic Inlet Duct Unstart Using Planar Laser Rayleigh Scattering," *Experiments in Fluids* (submitted for publication).

[25]Arai T., Sugiyama H., Abe F., Takahashi T., and Onodera O., "Internal Structure of Pseudo-Shock Waves in a Square Duct," Vol. 208, American Institue of Physics, College Park, MD, 1990, pp. 850 – 855.

[26]Hataue I., "Computational Study of the Shock-wave/boundary-layer Interaction in a Duct," *Fluid Dynamics Research*, Vol. 5, 1989, pp. 217-234.

[27]Katanoda H., Matsuoka T., and Matsuo K., "Experimental Study on Shock Wave Structures in Constant-area Passage of Cold Spray Nozzle," *Journal of Thermal Science*, Vol. 16, 2003, pp. 40-45.